

High-resolution transmission electron microscopy (HRTEM) investigation of antigorite polysomes ($m = 15$ to 18)

GIAN CARLO CAPITANI^{1,*} AND MARCELLO MELLINI²

¹Dipartimento Geomineralogico, Università di Bari, Via Orabona 4, 70125 Bari, Italy

²Dipartimento di Scienze della Terra, Università di Siena, Via Laterina 8, 53100 Siena, Italy

ABSTRACT

Single-crystal structure determinations of the $m = 17$ and $m = 16$ antigorite polysomes confirmed the existence of two basic antigorite structures, i.e., “odd” antigorites, with $m = 2n + 1$ (m being the number of tetrahedra in a wavelength visible in the [010] projections), and “even” antigorites, with $m = 2n$. Both structures contain “8-reversals” and “6-reversals.” The “8-reversals” consist of 8-member rings of tetrahedra, where four tetrahedra point in one direction and four in the opposite direction, whereas “6-reversals” involve four tetrahedra and two tetrahedra, respectively. “Odd” antigorites have m tetrahedra and $m - 1$ octahedra along a wavelength (which coincides with the a translation) and Pm space group. Conversely, $\mathbf{b}/2$ shifts every second 8-reversal cause the structure to be C -centered in “even” antigorites ($C2/m$ space group). In the latter case, m tetrahedra and $m - 1$ octahedra occur within a wave, but two waves occur within an a periodicity.

Transmission electron microscopy (TEM) of antigorite polysomes with m ranging from 15 to 18 is successfully interpreted on the base of previous X-ray data. In particular, [001] selected area electron diffraction (SAED) patterns show primitive or C -centered cells, for $m = 2n$ or $2n + 1$, respectively. In addition, [001] high-resolution (HR) images show 8-reversals aligned or offset by $\mathbf{b}/2$ (i.e., stacking based on a primitive or C -centered lattice).

Keywords: Antigorite, HRTEM, structure, polysomatism

INTRODUCTION

The antigorite polysomatic series (Spinnler 1985; Ferraris et al. 1986) has been investigated over the past 60 years by X-ray diffraction (e.g., Aruja 1945; Kunze 1956, 1958, 1960, 1961; Capitani and Mellini 2004, 2006) and transmission electron microscopy (e.g., Zussman et al. 1957; Yada 1979; Spinnler 1985; Uehara and Shirozu 1985; Mellini et al. 1987; Wu et al. 1989; Otten 1993; Viti and Mellini 1996; Uehara 1998; Dódony et al. 2002; Grobety 2003; Dódony and Buseck 2004; Capitani and Mellini 2005). Recently, the modulated crystal structures of two different antigorite polysomes, the $m = 17$ (Capitani and Mellini 2004) and the $m = 16$ (Capitani and Mellini 2006) were determined by single-crystal X-ray diffraction (SCXRD), using area detectors for intensity data acquisition and direct methods for the structure solution. These two polysomes differ in the numbers of [010] tetrahedral strips (17 vs. 16) and [010] octahedral strips (16 vs. 15) along the [100] modulation wave. They also differ in space group symmetries and in cell contents, but reveal very similar first neighbors interactions, that match the lizardite bonding geometry.

SCXRD structure determinations confirmed the electron diffraction data of Uehara and Shirozu (1985), who first suggested the existence of two basic antigorite modifications, i.e. “odd” antigorites, with $m = 2n + 1$ (m being the number of tetrahedra along a wavelength in [010] projections), and “even” antigorites, with $m = 2n$. Alternating 6-reversals (6-membered tetrahedral rings with four tetrahedra pointing along $+\mathbf{c}$ and two along $-\mathbf{c}$) and 8-reversals (8-membered tetrahedral rings with four tetra-

hedra pointing along $+\mathbf{c}$ and four along $-\mathbf{c}$) occur in both the antigorite modifications. “Odd” antigorites have m tetrahedra and $m - 1$ octahedra along a wavelength (which coincides with the a translation) and Pm space group. Conversely, $\mathbf{b}/2$ shifts every second 8-reversal cause the structure to be C -centered in “even” antigorites, which occur as $C2/m$ space group. For C -centered lattices, m tetrahedra and $m - 1$ octahedra occur within a wave, but two waves ($2m$ tetrahedra and $2m - 2$ octahedra) occur along a .

By means of high-resolution transmission electron microscopy, we investigate additional ordered antigorite polysomes, to show that those structural topologies occur also in polysomes with m other than 17 and 16. We also demonstrate full consistency between X-ray data, electron diffraction data, and HRTEM results for the $m = 16$ polysome.

SAMPLES AND EXPERIMENTAL TECHNIQUES

TEM mounts for [001] observations were prepared starting from the batch of crystals separated by Peretti (1988) and already used for single-crystal analyses by Capitani and Mellini (2004, 2006). TEM mounts for [010] observations were selected on petrographic thin sections of the hand specimen used by Peretti (1988). In both cases, electron transparency was achieved by standard ion milling techniques. Most of the TEM mounts are from the Mg159 sample and some from Mg63c; both samples are from the Val Malenco serpentinite body, but the latter formed at a lower metamorphic grade (Trommsdorff and Evans 1972; Mellini et al. 1987).

TEM investigations were performed at the University of Siena with a JEM2010 equipped with Fuji image plates. Before image processing and measurements, HR images and SAED patterns were corrected for projector lens distortion, following Capitani et al. (2005). Some SAED patterns along the [001] direction were acquired at Bari University with a JEM2010 equipped with a Gatan MSC 794 CCD detector (1k × 1k, 14 bit depth).

The program CRISP (v. 2.1a) by Calidris (www.calidris-em.com) was used to

* E-mail: g.capitani@geomin.uniba.it

measure cell constants and to remove the image blurring related to diffuse scattering that arises from electron-beam damage (during observation), ion-beam damage (during preparation), and carbon coating. This background noise was filtered out in the frequency domain by applying proper masks on the fast Fourier transforms (FFT) of the image and computing the inverse Fourier transform (IFT). For more details on this image processing, see Capitani and Mellini (2005). The program NCEMSS (v1.8) by Roar Kilaas (<http://ncem.lbl.gov/frames/software.html>) was used to calculate HR images and SAED patterns.

RESULTS AND DISCUSSION

The refined atomic coordinates of the $m = 16$ antigorite polysome (Fig. 1, after Capitani and Mellini 2006) were used to simulate SAED patterns and HR images. Whenever needed to allow comparison (especially to highlight differences between “even” and “odd” polysomes), simulations of the $m = 17$ polysome (Capitani and Mellini 2005; based upon atomic coordinates from Capitani and Mellini 2004) are provided as well.

SAED patterns

Projection along the [010] direction. Geometry and intensity distribution in the simulated [010] diffraction pattern for the $m = 16$ polysome qualitatively match the experimental pattern (Fig. 2). Minor differences arise because of the diffuse scattering around subcell reflections, possibly related to beam-damage effects. The strongest reflections cluster around $h = 15$ –16, rather than at $h = 16$ –17 as in the $m = 17$ polysome (Capitani and Mellini

2005), thus matching the different numbers of basic (tetrahedra, octahedra) polyhedra in the two superstructures. The measured projected cell constants are $a = 40.92$, $c = 7.25$ Å, $\beta = 91.4^\circ$, in agreement with the SCXRD values ($a = 81.664$, $b = 9.255$, $c = 7.261$ Å, $\beta = 91.409^\circ$; Capitani and Mellini 2006). The difference in a is related to systematic extinctions leading to apparent half values in the [010] projection. Although the half-superperiodicity value (and thus the m value, which is approximately $a/2.56$) may be measured, this diffraction net does not offer any feature distinguishing “even” from “odd” polysomes.

Projection along the [001] direction. Figure 3 shows the electron diffraction patterns along the [001] direction as calculated for the $m = 16$ and the $m = 17$ polysomes. Although similar at first glance, the $m = 16$ polysome (Fig. 3a) has a primitive oblique two-dimensional cell with $\gamma \approx 83.3^\circ$ (or, alternatively, a double C -centered rectangular cell), whereas the $m = 17$ polysome (Fig. 3b) has a primitive rectangular cell (upper right insets). Whereas 16,00 (oblique setting) is the strongest $h00$ reflection in the $m = 16$ polysome, 17,00 is the strongest in the $m = 17$ polysome. Thus, the [001] projection may be used to distinguish antigorite polysomes, by showing the primitive or centered nature of the lattice.

The experimental SAED pattern of the $m = 18$ polysome (Fig. 4a) shows the same geometrical features just described for the $m = 16$ polysome, differing in superperiodicity and strongest

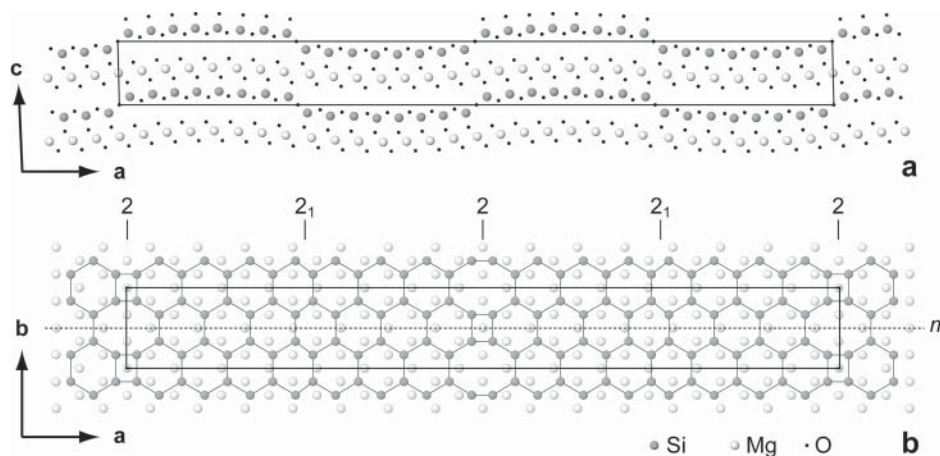


FIGURE 1. Crystal structure of the $m = 16$ antigorite polysome (Capitani and Mellini 2006) as seen along the [010] direction (a) and along the [001] direction (b). Hydrogen atoms are omitted in both figures. In addition, oxygen atoms are omitted in b.

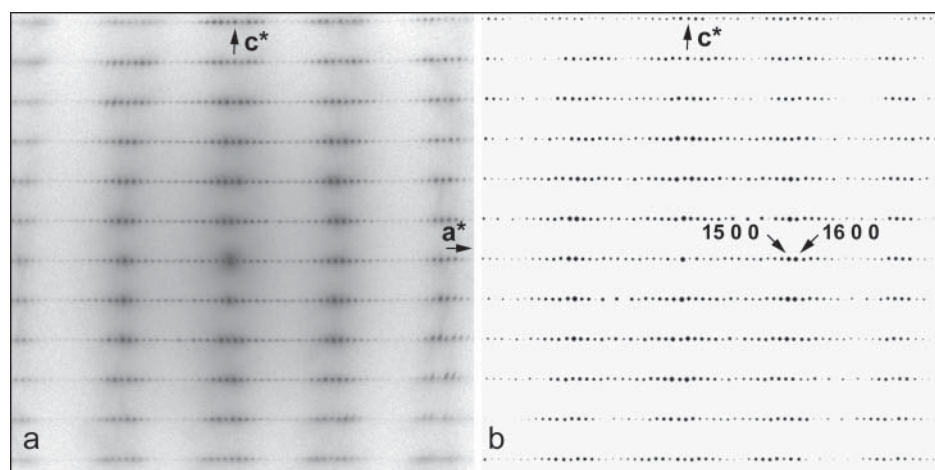


FIGURE 2. Experimental (a) and simulated (b) SAED patterns along the [010] direction of the $m = 16$ antigorite polysome. The diffracting area in a is about $20 \mu\text{m}^2$ (selected area diaphragm $5 \mu\text{m}$ in diameter). Simulation parameters: sample thickness, $t = 100$ Å; beam divergence, $\Delta = 0.1$ mrad.

$h00$ reflection (now 18,00). The measured cell parameters of the primitive oblique (o) setting ($a_o = 46.62$, $b_o = 9.20$ Å, $\gamma = 95.4^\circ$) transform to $a_r = 92.83$, $b_r = 9.20$ Å in the centered rectangular (r) setting.

For comparison, Figure 4b shows the experimental pattern of the $m = 17$ polysome acquired under similar experimental conditions. The primitive rectangular two-dimensional cell is evident, with 17,00 as the strongest $h00$ reflection. The measured cell parameters are $a = 43.50$, $b = 9.21$ Å. Therefore, this projection is more useful than the [010] in distinguishing antigorite polysomes by electron diffraction.

HRTEM images: the $m = 16$ polysome

Projection along the [010] direction. Simulated HR images (Fig. 5) of the $m = 16$ polysome do not show any major difference with respect to the $m = 17$ polysome (Capitani and Mellini 2005, Fig. 4), apart from the different numbers of white and black dots along a wave, and the presence of symmetry related halfwaves deriving from the $p2$ planar symmetry ($m = 16$), in place of $p1$ ($m = 17$). At Scherzer defocus and moderate thickness (20–60 Å), that is to say under weak-phase object approximation (WPOA), two rows of 16 ($m - 1$) white dots per wave alternate along c in the $m = 17$ polysome, whereas two rows of 15 white dots per wave alternate along c in the $m = 16$ polysome. Under WPOA, black dots correspond to atom columns, with 16 black dots per wave (corresponding to silicon atom columns) alternating along c with 15 black dots per wave (corresponding to magnesium atom columns) in the $m = 16$ polysome. In comparison there are 17 and 16 black dots per wave, respectively, for the $m = 17$ polysome.

In simulations along the [010] direction, 6-reversals and 8-reversals may be distinguished with difficulty by slightly different distributions of silicon-atom positions around reversal points. These distributions are characterized by a steeper offset along c for the 6-reversal, which derives from the $Mg(OH)_2$ depletion at reversal lines. In fact, depletion is accomplished for 2/3 of the octahedra at the 6-reversal and 1/3 of the octahedra at the 8-reversal, with total consumption of one octahedral [010] strip (Capitani and Mellini 2004, Fig. 5). However, this subtle difference cannot be recognized in the experimental HR images (Fig. 6), probably because of image blurring related to beam damage

or departure from ideal experimental conditions (e.g., crystal tilt, beam misalignment, astigmatism). For these reasons, the number of black dots cannot be unequivocally determined. In contrast, white dots are more evident, and their number in a wavelength is $m - 1$ in both rows, consistent with the simulated images.

Capitani and Mellini (2005) noticed on images taken along [010] that the antigorite superperiodicity appears distinct, whereas every-second halfwave periodicity appears blurred because of beam damage. Those authors assumed the distinct feature to be the 8-reversal, for consistency with HR images taken along the [001] direction. In fact, along this direction, the distinction between the two reversals is feasible, and the 8-reversal appears less affected by beam damage.

The average values of the unit-cell parameters measured on this HR image are $a = 41.00$, $c = 7.24$ Å, $\beta = 91.6^\circ$, as expected for the $m = 16$ polysome.

Projection along the [001] direction. Simulated [001] images of the $m = 16$ polysome for variable thickness at Scherzer defocus are reported in Figure 7. C -centering and the doubled a parameter are evident. The alternative primitive oblique two-dimensional setting does not emphasize the real symmetry of the structure (Capitani and Mellini 2006). Besides these characteristics and the different number of black (or white, depending upon thickness and defocus) dots in a wave, no local image-contrast difference occurs with respect to the $m = 17$ polysome, under similar experimental conditions (cf. Capitani and Mellini 2005, Fig. 7).

Because silicon atoms and apical oxygen atoms overlap in the [001] projection, these two atom types dominate the image-contrast. HR images along the [001] direction under WPOA conditions allow direct imaging of the silicon plus apical oxygen atom columns as arrays of black dots arranged in hexagonal rings. After contrast reversal at greater thickness or different defocus values, the rings may become white dots and possibly with additional white dots at the center of the rings (e.g., at 200 Å thickness). Figure 8 shows an ordered sequence of the $m = 16$ polysome. The enlargement of the central-left portion of the image shows 16 white dots per wave-forming hexagonal rings, plus 4-membered and 8-membered rings. Consistently, the FFT shows 16,00 as the strongest $h00$ reflection. The FFT planar symmetry is $c2mm$, as expected, with minor deviations possibly related to

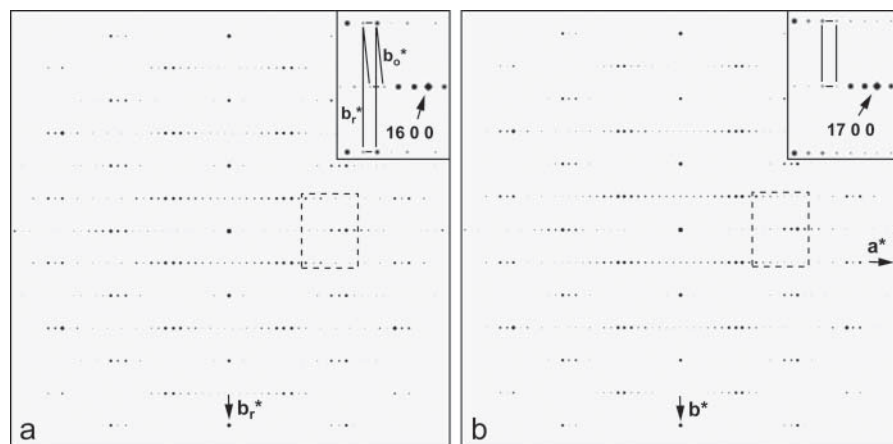


FIGURE 3. SAED simulations along the [001] direction ($t = 100$ Å; $\Delta = 0.1$ mrad). (a) $m = 16$ polysome. The primitive oblique and the centered rectangular two-dimensional cells are shown (upper right, enlargement of the dashed area; b_o^* = primitive oblique cell; b_r^* = centered rectangular cell). (b) $m = 17$ polysome showing a primitive rectangular cell (upper right inset). An intensity cut-off variable has been adjusted, and thus the figure differs from the calculated SAED of Capitani and Mellini (2005).

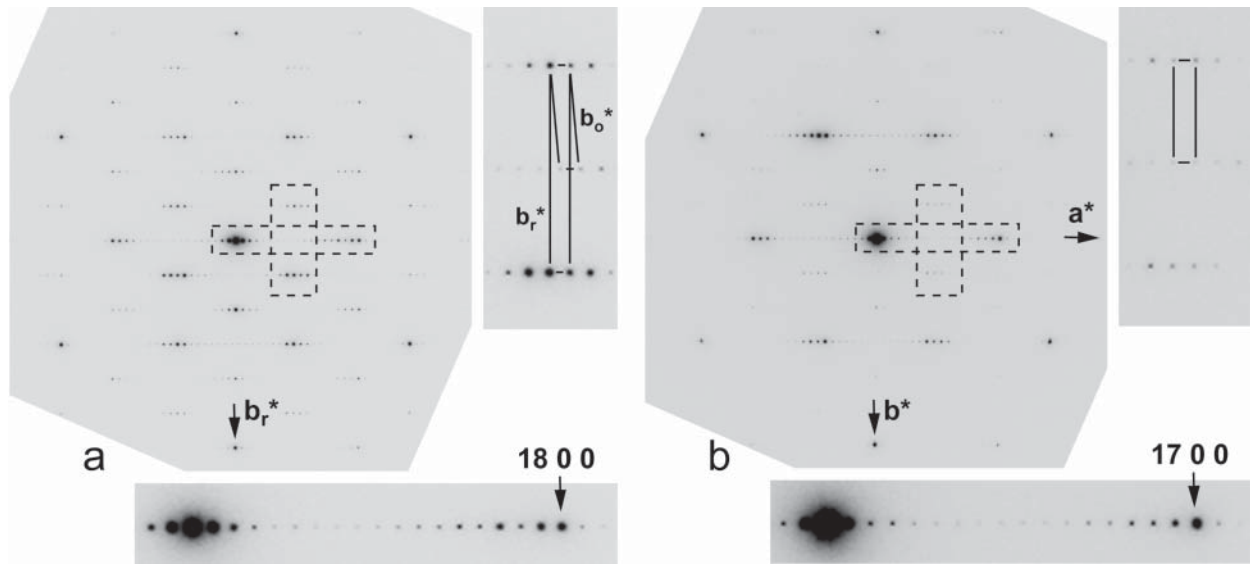


FIGURE 4. Experimental SAED patterns down the [001] direction. The diffracting area is about $3 \mu\text{m}^2$ (selected area diaphragm $2 \mu\text{m}$ in diameter). (a) $m = 18$ polysome. Note the primitive oblique two-dimensional cell and the alternative centered rectangular cell (right, enlargement of the dashed vertical region), as well as the strongest 18,00 reflection (bottom, enlargement of the dashed horizontal region). (b) $m = 17$ polysome. Note the primitive rectangular cell (right) and the strongest 17,00 reflection (bottom).

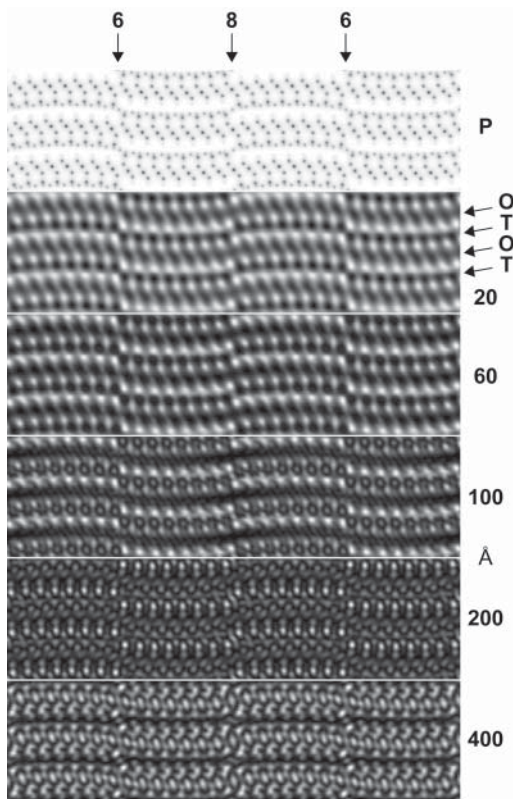


FIGURE 5. HR image simulations along the [010] direction of the $m = 16$ antigorite polysome (atomic coordinates from Capitani and Mellini 2006), for variable thickness (20 to 400 Å), at Scherzer defocus (-350 \AA), along with the projected potential (P). Simulation parameters: resolution, $Res = 2.0 \text{ \AA}$; spherical aberration, $C_s = 0.5 \text{ mm}$; chromatic aberration, $C_c = 1.1 \text{ mm}$; halfwidth of the Gaussian spread of focus, $S_f = 60 \text{ \AA}$; convergence semiangle, $\theta = 0.65 \text{ mrad}$.

crystal bending and/or crystal and/or beam misalignment. The cell constants measured from this image are $a_o = 40.93$, $b_o = 9.22 \text{ \AA}$, $\gamma = 96.6^\circ$ (oblique setting), transforming to $a_r = 81.32$, $b_r = 9.22 \text{ \AA}$ (centered rectangular setting). These values are slightly less than the parameters determined by SCXRD (probably owing to a $L\lambda$ camera constant less than assumed). Experimental images match the simulated images. The ill-defined bright strip laying along the 6-reversal line is related to beam damage. The $b/6$ offset of the subcell (130) plane at 8-reversals is evident in both the simulated and experimental images.

For comparison, we show an $m = 17$ polysome imaged under similar conditions. Seventeen white dots occur along a wave (Fig. 9). Consistently, 17,00 is the strongest $h00$ reflection in the FFT. No $b/2$ offset occurs between subsequent 8-reversals, but in the very right portion of the image, where an $m = 17$ lamella transforms to an $m = 18$ lamella from the top to the bottom of the image (note the switched position of white dot doublets along the 8-reversal line). Contrary to the $m = 16$ polysome, a rectangular primitive cell occurs with $a = 43.44$ and $b = 9.36 \text{ \AA}$, and this is consistent with the $m = 17$ polysome.

The $m = 18$ polysome

HRTEM investigations of the Mg159 sample show that $m = 17$ is the most abundant and the most commonly ordered polysome, but with $m = 16$ and $m = 18$ faults (Capitani and Mellini 2005). Ordered regions of the $m = 16$ polysome are not uncommon (as shown above), as well as of the $m = 18$ polysome (as hereafter reported).

Projection along the [010] direction. Contrast on HR images down the [010] direction of the $m = 18$ polysome under optimal conditions is dominated by two wavy rows of dots extending along a and alternating along c (Fig. 10; cf. to Fig. 6, and to Figs. 5 and 6 in Capitani and Mellini 2005). The number of white dots

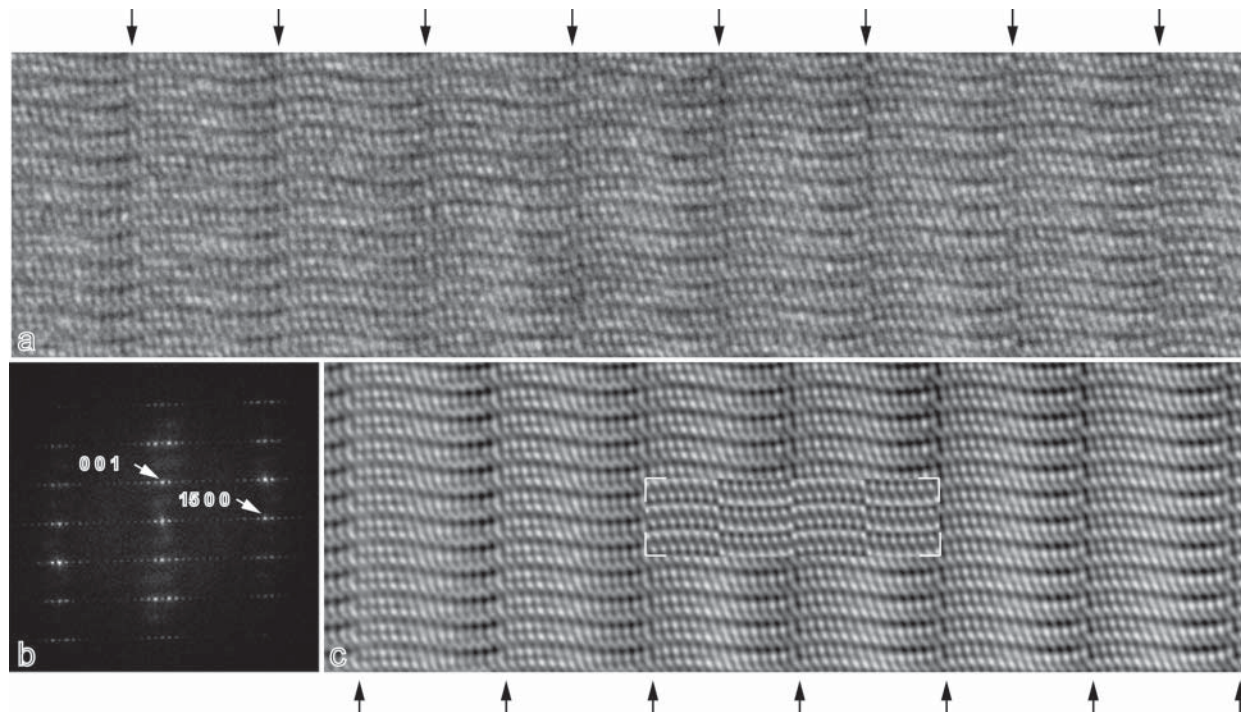


FIGURE 6. HR image down the $[010]$ direction of an $m = 16$ polysome. (a) As acquired image. (b) Corresponding FFT. Strongest reflections cluster around $\langle 15,0/t \rangle$ and $\langle 00/t \rangle$. (c) IFT along with the simulation (inset) at $\Delta_y = -350 \text{ \AA}$, and $t = 60 \text{ \AA}$. Outer arrows indicate the (supposed) 8-reversal positions (spaced apart about 41 \AA).

along each wave is $m - 1$, consistent with the images calculated under WPOA (Fig. 5, this paper, and Fig. 4 in Capitani and Mellini 2005). In contrast, black dots are ill-defined and one row is more distinct than the other, suggesting higher electron density. Also, the black dots are poorly resolved, and the steep offset at 6-reversal is not apparent.

A note on the apparent local cell variation. The average values of the unit-cell parameters measured on this HR image are $a = 46.23$, $c = 7.32 \text{ \AA}$, $\beta = 93.0^\circ$. Although the a parameter is consistent with the $m = 18$ polysome (i.e., $46.23/2.56 = 18.06$), the c -axis and the β -angle values are significantly higher than the values expected for antigorite. We find an apparently significant local variation of the cell parameters as function of distance of the measured area from the sample rim, i.e., the thickness of the thin foil. In this example, Figure 10 refers to a relatively thin area recorded at the corner of the image plate (the related cell parameters are those reported above). The cell parameters measured on a thicker area at the center of this same image plate are $a = 46.16$, $c = 7.23 \text{ \AA}$, $\beta = 91.5^\circ$, which match to the expected values. Perhaps, the apparent lattice-parameters variation is related to crystal effects or to detection effects. In the first case, we would expect a bent crystal rim, either deformed under its own weight and/or electron beam pressure; in the second case, bent image plate on the supporting devices.

Projection along the $[001]$ direction. HR images of the $m = 18$ polysome show the expected C -centered rectangular two-dimensional cell (Fig. 11). Average cell parameters for this setting are $a = 91.98$, $b = 9.31 \text{ \AA}$, $\gamma = 90^\circ$. Eighteen white dots occur along a wave, and 18,00 is the strongest $h00$ reflection. With respect to our previous HR images along the $[001]$ direc-

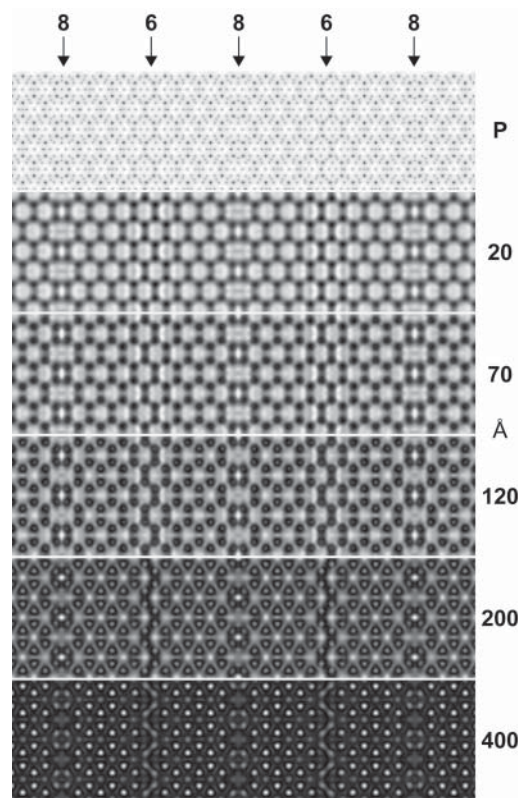


FIGURE 7. HR image simulations down the $[001]$ direction of an $m = 16$ polysome along with the projected potential. Simulations parameters as in Figure 2.

tion, the resulting image shows the white dots at the center of the tetrahedral rings and not the tetrahedral rings themselves, making the (110) subcell planes (as defined by Uehara 1998) more evident than the (130) planes. The $b/2$ offset of these planes at 8-reversal positions is readily recognizable, and the $b/2$ shift of every second 8-reversal is also clear.

The $m = 15$ polysome

Sample Mg159 does not have ordered regions or faults of polysomes other than $m = 16-18$. HRTEM investigations on other samples, still from Val Malenco but collected at different locations (at distances further from the pluton; Mellini et al. 1987), are composed of mostly disordered crystals, but in one

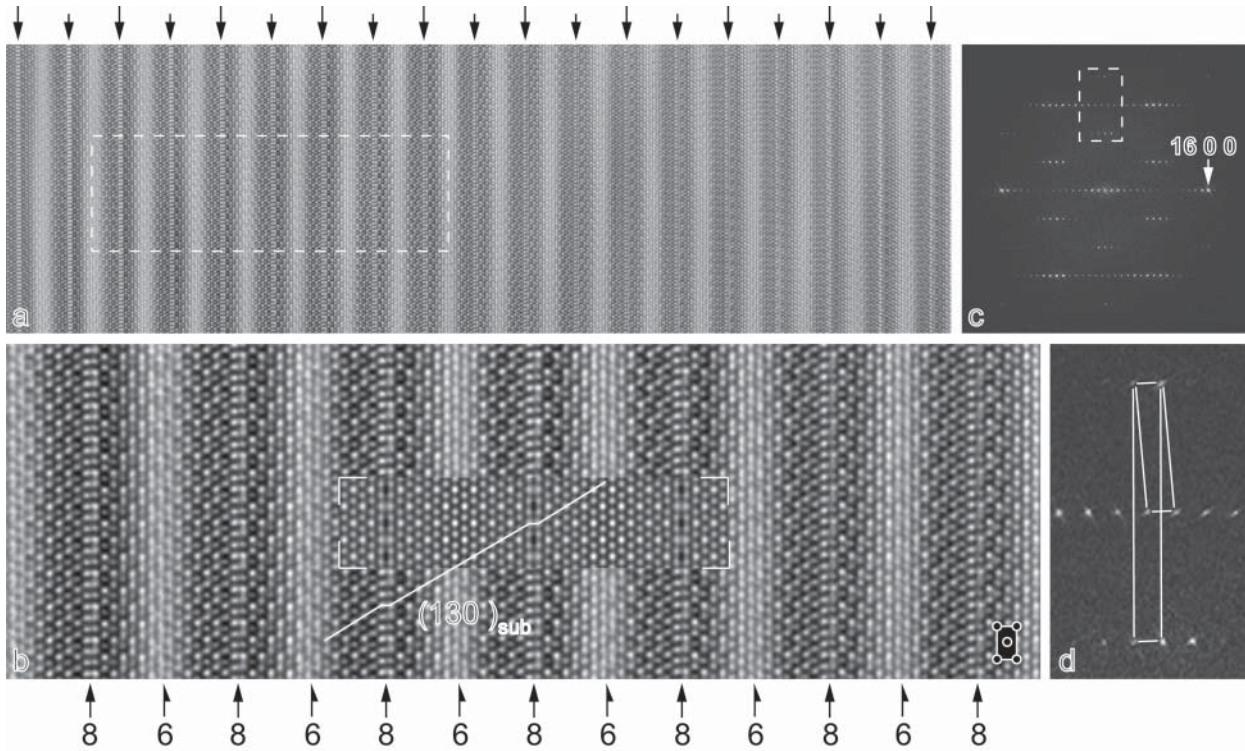


FIGURE 8. HR image down the [001] direction of an $m = 16$ polysome. (a) IFT image of a wide-ordered region. Top arrows indicate 8-reversal lines. Long and short arrows emphasize the $b/2$ shift of every second 8-reversal position and the consequent doubling of the lattice parameter. (b) Enlargement of the region dashed in a, along with image simulation (inset). The latter was obtained for a $\Delta_r = -100 \text{ \AA}$ and $t = 60 \text{ \AA}$. 8-reversal (2-diad axis) and 6-reversal (2₁-screw axis) positions are indicated. Note the $b/6$ offset of (130) subcell planes at 8-reversal positions (the rectangular subcell, about $5 \times 9 \text{ \AA}$, is shown at the bottom right). (c) FFT of the (a) image. Note the strongest 16,00 reflection. (d) Enlargement of the dashed area indicated in c. The primitive oblique and the centered rectangular two-dimensional reciprocal cells are shown (solid lines).

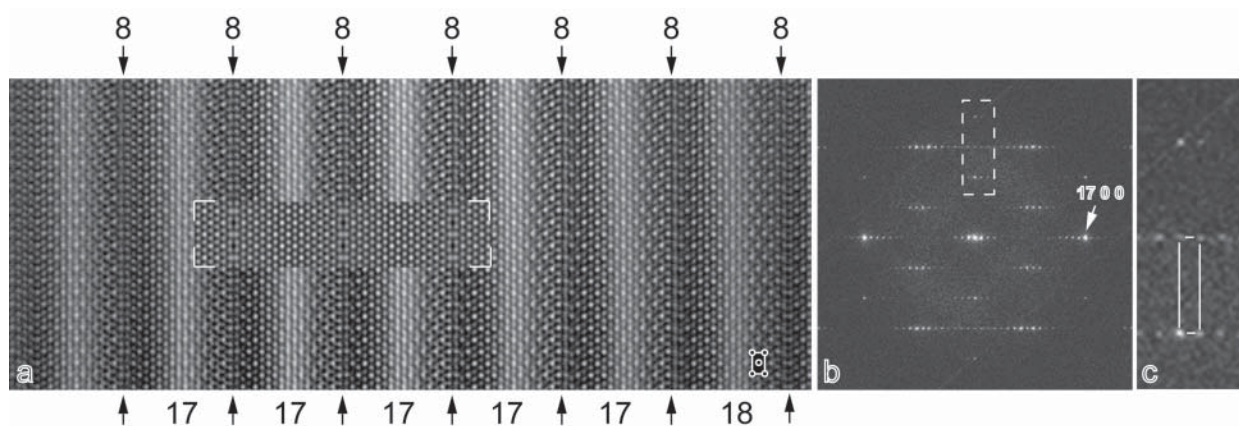


FIGURE 9. HR image down the [001] direction of an $m = 17$ polysome. (a) IFT image along with simulated image (inset). Simulation parameters as in Figure 2. The 8-reversal positions (arrows) and the polysome m number (bottom) are indicated, as well as the $5 \times 9 \text{ \AA}$ rectangular subcell (bottom right side); (b) FFT of a. Note the strongest 17,00 reflection. (c) Enlargement of the dashed area indicated in b. The primitive rectangular cell is shown (solid line).

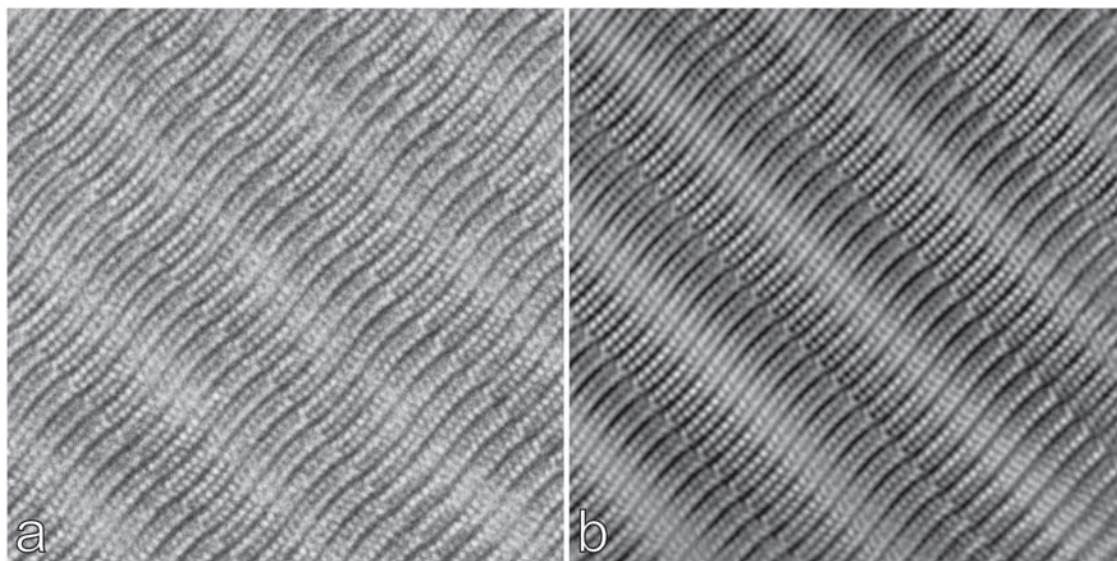


FIGURE 10. HR image down the [010] direction of an $m = 18$ polysome. (a) As acquired image. (b) Corresponding Fourier-filtered image (supercell periodicity about 46 Å).

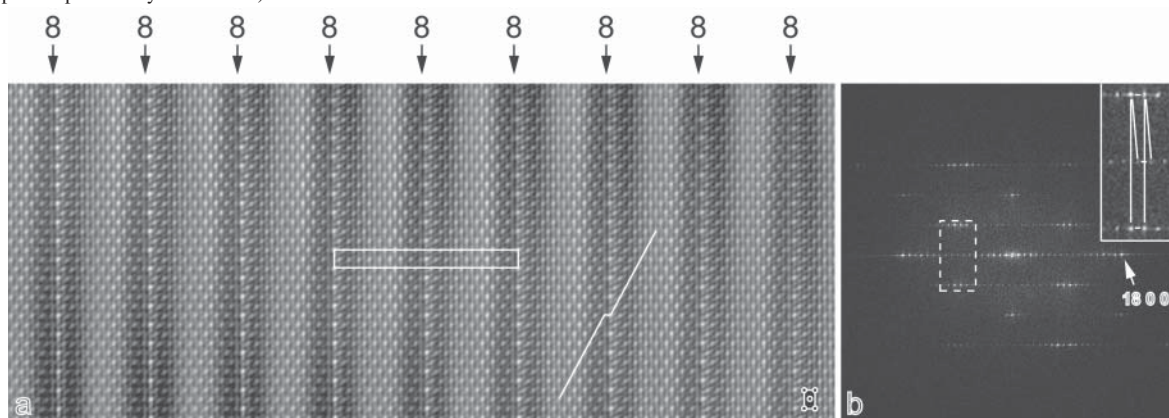


FIGURE 11. HR image down the [001] direction of an $m = 18$ polysome. (a) IFT image showing the C -centered rectangular two-dimensional cell and the $b/2$ offset of the subcell (110) planes at 8-reversal lines (the 5×9 Å subcell is shown at the bottom right side). (b) FFT of a. Note the strongest 18,00 reflection and the two possible cell settings (inset, enlargement of the dashed region).

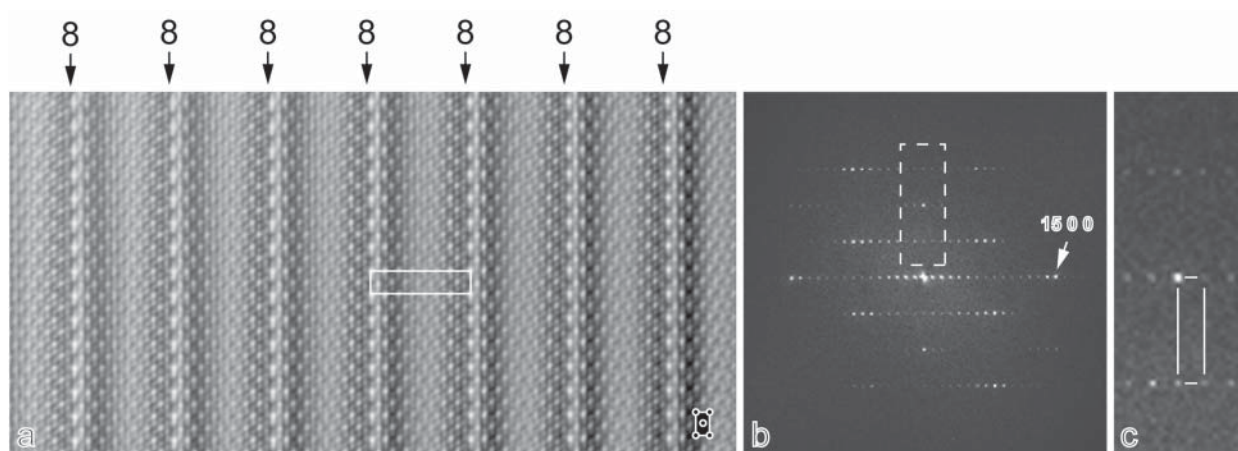


FIGURE 12. HR image down the [001] direction of an $m = 15$ polysome. (a) IFT image showing the primitive rectangular two-dimensional cell (the 5×9 Å subcell is shown at the bottom right side). With respect to the previous [001] images, the current image was acquired at low magnification and suffers of significant misalignment, as testified by the FFT (b). However, despite non-optimal conditions, 15 white dots occur along a and 15,00 is the strongest reflections. (c) Enlargement of the dashed region in b clearly showing the primitive rectangular cell.

case (Mg63c), a near ordered crystal of the $m = 15$ polysome was found. As expected, HR images along the [001] direction and the related FFTs show a primitive rectangular two-dimensional cell (Fig. 12). Consistently, 15 white dots occur along a , and 15,00 is the strongest $h00$ reflection. The measured cell parameters are $a = 38.02$, $b = 9.25$ Å, $\gamma = 90.0^\circ$, which are consistent with the $m = 15$ polysome (i.e., $38.02/2.56 = 14.85$).

ACKNOWLEDGMENTS

G.C.C. is indebted to S. Hovmöller and P. Oleynikov for their kind hospitality during the permanence at the Department of Structural Chemistry of Stockholm University and for deep training into the program CRISP. Suggestions by I. Dódney, S. Uehara, and S. Guggenheim greatly improved the original manuscript.

REFERENCES CITED

- Aruja, E. (1945) An X-ray study of the crystal structure of antigorite. *Mineralogical Magazine*, 27, 65–74.
- Capitani, G.C. and Mellini, M. (2004) The crystal structure of antigorite: the $m = 17$ polysome. *American Mineralogist*, 89, 147–158.
- — — (2005) HRTEM evidence for 8-reversals in the $m = 17$ antigorite polysome. *American Mineralogist*, 90, 991–998.
- — — (2006) The crystal structure of a second antigorite polysome ($m = 16$), by single-crystal synchrotron diffraction. *American Mineralogist*, 91, 394–399.
- Capitani, G.C., Oleynikov, P., Hovmöller, S., and Mellini, M. (2005) A practical method to detect and correct for lens distortion in the TEM. *Ultramicroscopy*, 106, 66–74.
- Dódney, I. and Buseck, P.R. (2004) Serpentine close-up and intimate: An HRTEM view. *International Geology Review*, 46, 507–527.
- Dódney, I., Pósfai, M., and Buseck, P.R. (2002) Revised structure models for antigorite: An HRTEM study. *American Mineralogist*, 87, 1443–1457.
- Ferraris, G., Mellini, M., and Merlino, S. (1986) Polysomatism and the classification of minerals. *Rendiconti della Società Italiana di Mineralogia e Petrografia*, 41, 181–192.
- Grobély, B. (2003) Polytypes and higher-order structures of antigorite: A TEM study. *American Mineralogist*, 88, 27–36.
- Kunze, V.G. (1956) Die gewellte Struktur des Antigorits, I. *Zeitschrift für Kristallographie*, 108, 82–107.
- — — (1958) Die gewellte Struktur des Antigorits, II. *Zeitschrift für Kristallographie*, 110, 282–320.
- — — (1960) Electron diffraction and moiré-patterns of the waved superlattice of antigorite. *Acta Crystallographica*, 13, 1093–1094.
- — — (1961) Antigorit. *Fortschritte der Mineralogie*, 39, 206–324.
- Mellini, M., Trommsdorff, V., and Compagnoni, R., (1987) Antigorite polysomatism: behaviour during progressive metamorphism. *Contribution to Mineralogy and Petrology*, 97, 147–155.
- Otten, M.T. (1993) High-resolution electron microscopy of polysomatism and stacking defects in antigorite. *American Mineralogist*, 78, 75–84.
- Peretti, A. (1988) Occurrence and stability of opaque minerals in the Malenco serpentinite. Ph.D. Dissertation, Eidgenössische Technische Hochschule (ETH), Zürich.
- Spinnler, G.E. (1985) HRTEM study of antigorite, pyroxene-serpentine reactions and chlorite, 248 p. Ph.D. thesis, Arizona State University, Tempe.
- Trommsdorff, V. and Evans, B.W. (1972) Progressive metamorphism of antigorite schist in the Bergell tonalite aureole (Italy). *American Journal of Science*, 272, 423–437.
- Uehara, S. (1998) TEM and XRD study of antigorite superstructures. *Canadian Mineralogist*, 36, 1595–1605.
- Uehara, S. and Shirozu, H. (1985) Variations in chemical composition and structural properties of antigorites. *Mineralogical Journal*, 12, 299–318.
- Viti, C. and Mellini, M. (1996) Vein antigorite from Elba Island, Italy. *European Journal of Mineralogy*, 8, 423–434.
- Wu, X.J., Li, F.H., and Hashimoto, H. (1989) High-resolution transmission electron microscopy study of the superstructure of Xiuyan Jade and Matterhorn serpentinite. *Acta Crystallographica*, B45, 129–136.
- Yada, K. (1979) Microstructures of chrysotile and antigorite by high-resolution electron microscopy. *Canadian Mineralogist*, 13, 227–243.
- Zussman, J., Brindley, G.W., and Comer, J.J. (1957) Electron diffraction studies of serpentine minerals. *American Mineralogist*, 42, 133–153.

MANUSCRIPT RECEIVED DECEMBER 13, 2005

MANUSCRIPT ACCEPTED AUGUST 14, 2006

MANUSCRIPT HANDLED BY STEPHEN GUGGENHEIM